buildings

MDPI

Article

Application of FEM and Artificial Intelligence Techniques (LRM, RFM & ANN) in Predicting the Ultimate Bearing Capacity of Reinforced Soil Foundation

Pandi Anandhi Jeyaseelan * and Muttharam Madhavan

Division of Soil Mechanics and Foundation Engineering, Department of Civil Engineering, College of Engineering Guindy, Anna University, Chennai 600025, India; muttharam@annauniv.edu
* Correspondence: pandianandhi.j@gmail.com

Abstract: In this research paper, the behavior of shallow footing with square and rectangular shapes over geosynthetic reinforced soil was studied. A novel geogrid called "3D tube-geogrid" was utilized for this work. The impact of various reinforcement parameters, including the depth of the final layer (z), length (l), inclination (α), filler material used inside the geogrid tube, relative soil density, and the tensile stiffness of the geogrid (EA), were analyzed by running numerical simulations using PLAXIS 3D V20 software. The simulated data were used to quantify the relationship between the ultimate bearing capacity of the soil and the reinforcement parameters. Several artificial intelligence (AI) techniques, such as linear regression analysis, a random forest model, and an artificial neural network (ANN), were employed on the generated dataset. To evaluate the preciseness of these techniques, various statistical indicators, such as the squared correlation coefficient (R^2), mean absolute percentage error (MAPE), mean squared error (MSE), and root-mean-square error (RMSE), were calculated, and error percentages of 20.98%, 12.5%, and 6.4% were obtained for the linear regression, random forest, and ANN, respectively. The numerical study determined the optimal values of the reinforcement parameters length, z/B, inclination, and filling material to be 4B, 3, 0°, and aggregate, respectively.

Keywords: geogrid; ultimate bearing capacity (UBC); PLAXIS; artificial intelligence (AI)

check for updates

Citation: Jeyaseelan, P.A.; Madhavan, M. Application of FEM and Artificial Intelligence Techniques (LRM, RFM & ANN) in Predicting the Ultimate Bearing Capacity of Reinforced Soil Foundation. *Buildings* **2024**, *14*, 2273. https://doi.org/10.3390/buildings14082273

Academic Editor: Eugeniusz Koda

Received: 14 June 2024
Revised: 13 July 2024
Accepted: 18 July 2024
Published: 23 July 2024

Copyright: © 2024 by the authors. Licensee MDPI, Basel, Switzerland. This article is an open access article distributed under the terms and conditions of the Creative Commons Attribution (CC BY) license (https://creativecommons.org/licenses/by/4.0/).

1. Introduction

Geosynthetics are typically employed to perform tasks such as separation, reinforcement, drainage, or filtration; they are manufactured from several kinds of polymers. The most prominent geosynthetic materials are geotextiles, geogrids, geomembranes, geosynthetic clay liners, and geonets. In the past 50 years, there has been a major advancement in the study and use of geosynthetics as reinforcements in the form of reinforced soil earth structures. The primary purpose of reinforcement is to increase the tensile strength of the soil by mobilizing the passive resistance along the transverse ribs and the frictional resistance on the reinforcement [1–3]. To improve our grasp of the mechanisms underlying geosynthetic–soil interactions, numerous experimental studies have been conducted [4–14].

Because of the difficulty in conducting multiple experiments at a large scale or in laboratories, researchers have begun to depend on software for predicting the UBC of the reinforced soil bed. In the design of foundations, UBC is the most essential factor; hence, it is critical to study the effects of geosynthetics on UBC. Various numerical experiments have been conducted using software such as FLAC 2D 8, GEOSTUDIO V 7.10, PLAXIS 3D V8, etc. The authors [15] studied the effects of eccentric and oblique loading on a rectangular footing on geogrid-reinforced sand; the research was conducted using PLAXIS 3D, and the results showed that the UBC increased by 75% for multiple geogrid layers. The authors of [16] investigated the effect of geogrid layers on the UBC of soil on circular footing; this study focused on identifying the optimal values of geometric factors, such as

the length of the geogrid, the number of layers, the spacing between the layers, the distance between the footing and the geogrid reinforcements, and the depth of the footing, using PLAXIS 2D. The results showed a 50% increase in the bearing capacity ratio (BCR) for the optimal values. The impact of interlaced geotextile reinforcement with wrapping around the geotextile was studied by [17] using PLAXIS 2D. The outcome showed that by using the wrap-around ends, the UBC of the soil and the stiffness of the sand bed increased in terms of the modulus of the subgrade reaction. Additionally, this saves land space for the construction of reinforced soil. The authors of [18] assessed the UBC of the footing on a geosynthetic-reinforced sand bed using the computer program FLAC^{3D}, as well as studied the impacts of different reinforcement parameters on UBC, such as the type and tensile strength of the geosynthetic material, the number of reinforcements, and the configuration of the geosynthetic layers below the footing. It has been noted that the layout and the pattern of the reinforcement are crucial in improving the UBC. Using PLAXIS 2D, ref. [19] examined the load-settlement behavior of strip footing on a reinforced sand bed. The experiments were conducted with densities ranging from moderately dense to very dense. The results emphasized that, with an increase in the embedment depth and the UBC, in the presence of wrap-around ends, the stiffness of the soil increases. The load-settlement behavior of a circular footing containing prestressed geosynthetics was analyzed using PLAXIS Version 8 [20]. The results showed that, by adding the prestressed reinforcement, the settlement of the soil reduced, while the UBC of the soil improved. The authors [21] studied the effects of rotational and horizontal constraints of strip footings placed adjacent to one another on granular soil using PLAXIS 2D and Optum G2. The results indicated that constraining the horizontal and rotational movement of the footing increases the UBC.

Subsequently, over the past 10 years, the modeling of geotechnical problems using modern techniques in machine learning and artificial intelligence has been increasingly adopted in several studies. Many attempts have been made using different machine learning techniques to predict the bearing capacity [22–28]. The authors [29] deployed several machine learning techniques based on genetic algorithms, gradient-based algorithms, and neural networks to predict UBC given several parameters. The results predicted by AI-based techniques generated ultimate bearing capacity equations that provided above 90% accuracy, with ANNs surpassing other methodologies. The authors [30] proposed a new technique to predict the settlement of the footing on sand beds with geosynthetic reinforcements; they used a combination of optimization and neural network referred to as the "Artificial Neural Network—Grey Wolf Optimization" model. The study also claimed that the developed model could reliably predict the footing settlement and, hence, could be used for the design of footing on geosynthetic-reinforced soil. The impacts of multidirectional reinforcement elements on the UBC of sand beds were analyzed [31]. The empirical study suggested that having four layers with a spacing of 0.5 B nearly tripled the UCB of the soil. An ANN model was trained to predict the UBC given the reinforcement parameters. The authors [32] predicted the ultimate bearing capacity using an optimized artificial neural network (ANN), a genetic algorithm optimized with ANN (GA-ANN), particle swarm optimization optimized with an ANN (PSO-ANN), a differential evolution algorithm (DEA), an adaptive neuro-fuzzy inference system (ANFIS), a general regression neural network (GRNN), and a feedforward neural network (FFNN). The AI techniques have several advantages over conventional methods, chief among them being their capacity to derive knowledge from observed data without presumptions. This ability makes these approaches very appropriate for mapping the nonlinear relationships between input and output variables.

The extensive literature review identified the usage of geocells and wrap-around ends of geogrids as reinforcement. Nevertheless, no direct research has been conducted on the role of tubular geogrids in the design of reinforced soil structures. Therefore, an attempt is made in this research to study and evaluate the effect of tubular geogrids as reinforcements to increase the bearing capacity of soil by conducting numerical simulations using PLAXIS 3D. These simulations were validated using several laboratory tests. In

addition to this, AI techniques such as an artificial neural network (ANN), random forest model, and linear regression were used to predict the UBC of the reinforced sand bed. Equations were also created from the generated model for simple manual computations and preliminary requirements in design. This will assist in reducing the time and resources (both computational and financial) needed to complete numerical simulations and model plate load tests. The primary objective of this study is to present and prove the usage of 3D tube geogrids as a soil-reinforcing material for various geotechnical applications, such as footings and roadbed construction.

2. Methodology

The simulations were carried out on two different shapes of footing: a square footing of 100 mm, and a rectangular footing of 100 × 150 mm. A new form of reinforcement obtained by rotating the geogrid into a tubular shape was also used for the study. The modeling was performed by altering the depth of the final layer of the tubular geogrid (z/B = 1.5, 3, or 4.5), the length of the tubular geogrid (l/B = 3, 4, or 5), the angle of inclination of the tubular geogrid ($\alpha = 0^\circ$, 90°, or 120°), the type of filler inside the tubular geogrid (sand or aggregate), the relative density of the sand (30%, 45%, 60%, 75%, or 90%), and different types of geogrid (EA = 500 kN/m, 800 kN/m, or 1144 kN/m).

3. Numerical Analysis

Of all the numerical methods, the FEM (finite element method) was chosen to model the settlement behavior based on the vast literature survey and its researcher-friendly nature. The FEM can easily represent many sorts of material properties from element to element, and it can also quickly integrate boundary conditions. Here, numerical simulations were carried out using the PLAXIS 3D package.

The soil mass is assumed to be homogeneous, isotropic, and perfectly plastic; additionally, it obeys the "Mohr–Coulomb" failure criterion and associated flow rule. The properties of the geosynthetic materials are provided in Table 1. Three different types of geogrids were used for the tests. Similarly, the properties of the soil are provided in Table 2.

Table 1. Properties of geogrids.

Type	Shape of Aperture	Size of Opening (mm × mm)	Thickness of Mesh (mm)	Tensile Strength (kN/m)	Tensile Stiffness (kN/m)
Geogrid 1	Oval	6 × 8	2.8	25	500
Geogrid 2	Oval	8 × 9	3.0	27.4	800
Geogrid 3	Oval	10 × 10	3.1	31.5	1144

Table 2. Soil properties.

Parameter	Value
Material	Sand
Bulk unit weight, γ (kN/m^3)	16.97
Saturated unit weight, γ_{sat}(kN/m^3)	20.07
Elastic modulus of sand, E (kN/m^2)	45×10^3
Poisson's ratio, υ	0.33
Cohesion, c (kPa)	1

For soil modeling, a 15-node triangular element with 12 stress points was employed. Five nodes were used to model the geogrid. A geometric model was constructed with dimensions of 1.00 m × 0.60 m × 0.60 m(L × B × H).

Fixed boundary conditions were innately applied to the boundaries. Furthermore, the sand was assigned a cohesion value of 1.0 kPa, and the angle of dilation (Ψ) was determined using Bolton's relationship as expressed as $\Psi \cong \phi - 30^{\circ}$. The footing was designed as an isotropic plate element, and the unit weight of steel was given as 78.5 kN/m^3, with geogrid elements as reinforcements. The same degree of roughness was given to the upper and lower surfaces of the reinforcements. The walls of the container were assumed to be rigid. The interfaces were assigned a rigid setting corresponding to R_{inter} = 1.0. Following a sensitivity analysis, a fine-sized mesh was used for model simulations. To minimize the effect of meshing, a prescribed displacement option was used to apply the settlement. Figure 1a shows the model footing on the soil, and Figure 1b shows the soil with multiple layers of tubular geogrid.

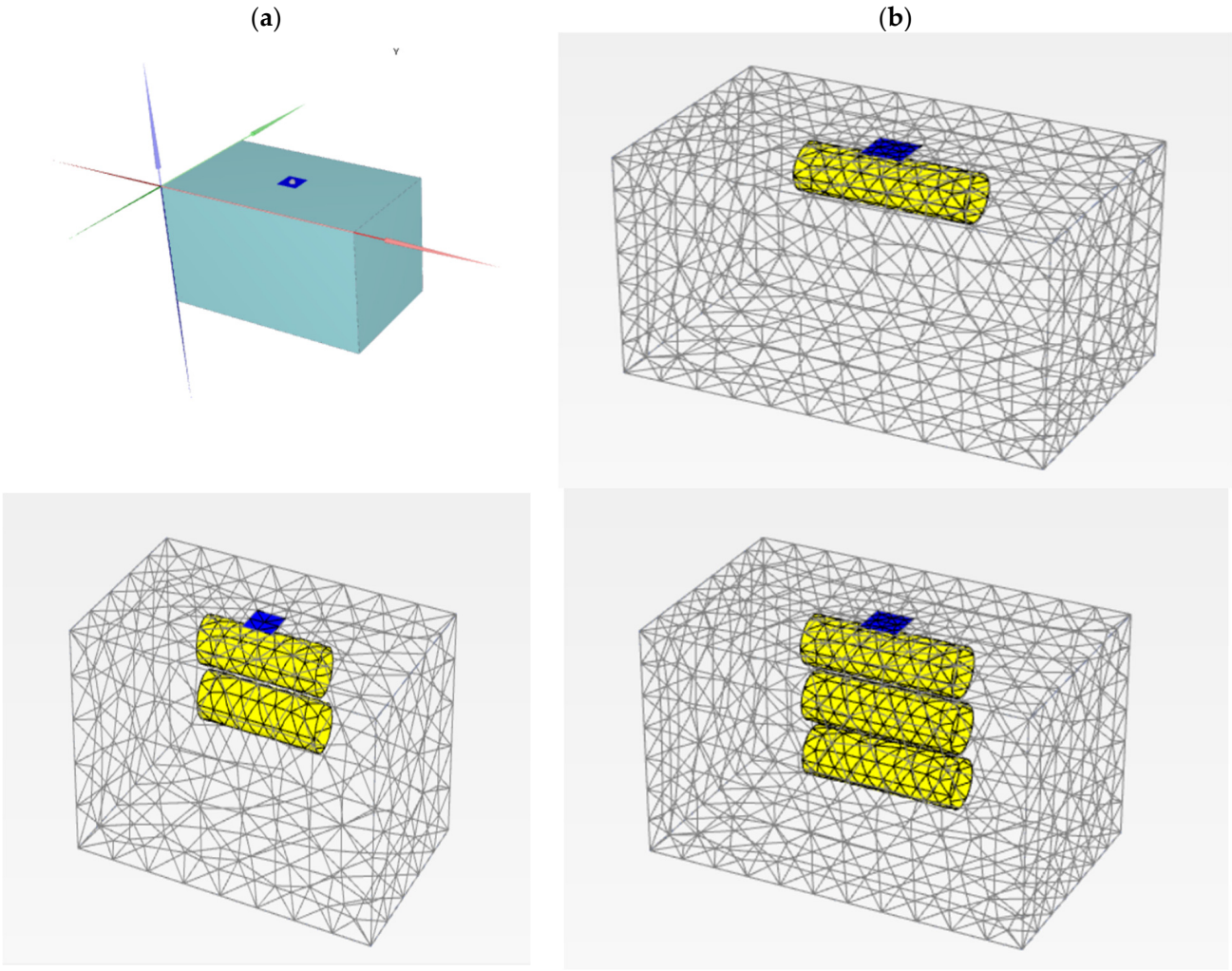


Figure 1. (**a**) Model footing on soil; (**b**) model with multiple layers of tubular geogrid.

4. Results and Discussion

The unreinforced sand bed model was developed based on the specified parameters, and the calculations were carried out. The ultimate bearing capacity obtained for a 25 mm settlement was 188.1 kN/m^2 for square footing and 193.33 kN/m^2 for rectangular footing.

4.1. The Impact of the Depth of the Final Layer of the Tubular Geogrid (z)

Analysis was conducted by altering the final depth of the reinforcement (z) between 1.5 and 4.5 B. Other parameters, such as the length of the tubular geogrid, inclination, filling inside the geogrid, relative density, and the stiffness of the geogrid were kept constant at 4 B, 0°, sand, 45%, and 1144 kN/m, respectively. Figure 2 shows the variation in BCR with

the depth of the final layer of the tubular geogrid (z/B) for both square and rectangular footing, where BCR is the bearing capacity ratio, which is the ratio of the ultimate bearing capacity of reinforced soil ($q_{u\ reinforced}$) to the ultimate bearing capacity of unreinforced soil ($q_{u\ unreinforced}$).

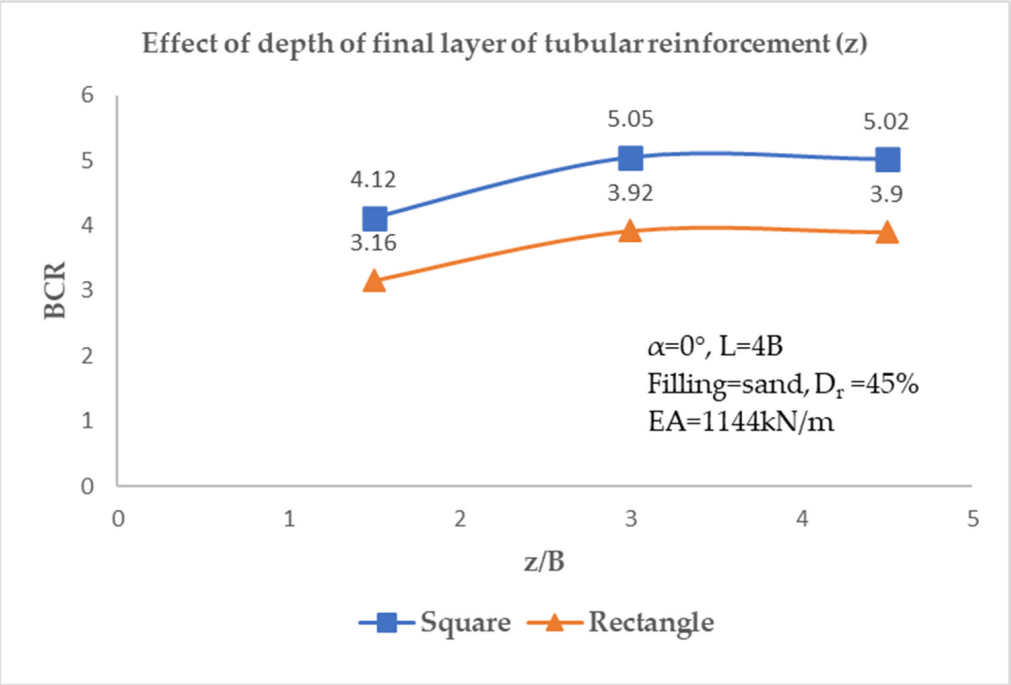


Figure 2. BCR versus z/B for square and rectangular footing.

It can be seen from the graph that, as the depth of the final layer increases, the BCR increases until 3 B and then decreases at 4.5 B for both rectangular footing and square footing. The maximum BCR was obtained for square footing with a total reinforcement depth of 3 B (footing width). Increasing the depth beyond 3 B will not make much difference to the BCR and will also not be cost-effective. When increasing the depth of the final layer, multiple layers of the tubular geogrids are introduced in between. The confinement effect created by the soil in between the layers and inside the tubular shape contributes to the increase in the UBC.

4.2. Impact of Inclination of Tubular Geogrid (α)

Numerical analysis of the effect of the inclination of the tubular geogrid was carried out by varying the inclination (0°, 90°, and 120°) with respect to the length of the sand bed, keeping the length of the geogrid, filling, relative density, and the stiffness of the geogrid constant at 4 B, sand, 45%, and 1144 kN/m, respectively. The depth to the final layer of the tubular geogrid was also varied for each trial. Figure 3 shows the BCR variations for different inclinations. The increase in bearing capacity was not much different for 0° and 90°, but for 120°, the analyses showed lesser values of UBC than the other inclination angles.

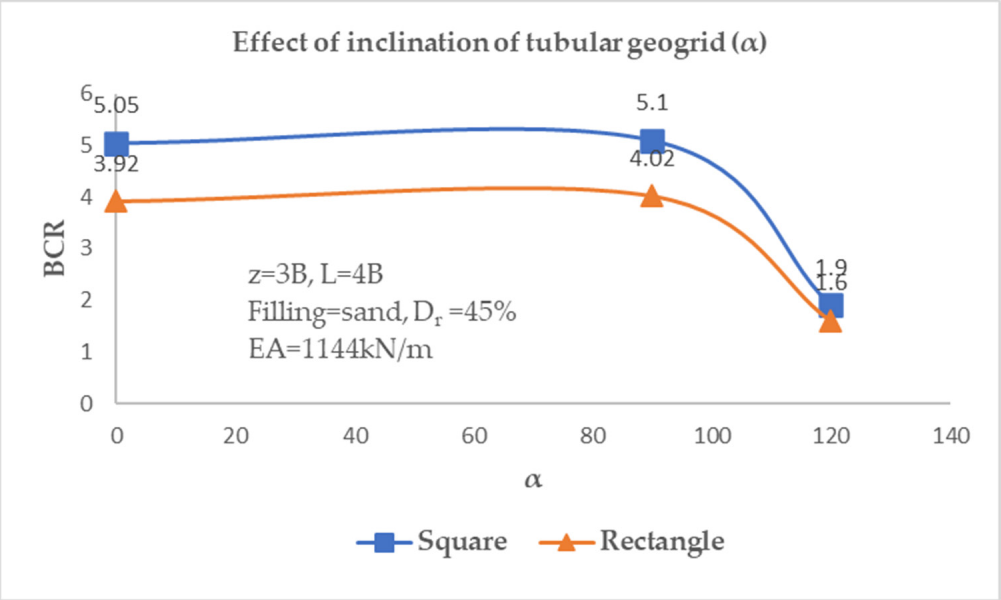


Figure 3. BCR versus α for square and rectangular footing.

4.3. The Impact of the Length of the Tubular Geogrid (L)

For analyzing the impact of the length of the tubular geogrid, the length was varied (3B, 4B, and 5B) while keeping the depth to the final layer, inclination, filling material, relative density of sand, and the stiffness of the geogrid constant at 3 B, 0°, sand, 45%, and 1144 kN/m, respectively. Based on Figure 4, when the length of the geogrid increases, the UBC also increases. UBC values as high as 900 kN/m^2 were obtained for rectangular footing. Increasing the length to more than 5 B would not be cost-effective. Thus, when the reinforcement length is $3 \geq L \leq 5$, the reinforced soil performs at its best. This is consistent with the suggested size according to [33–35].

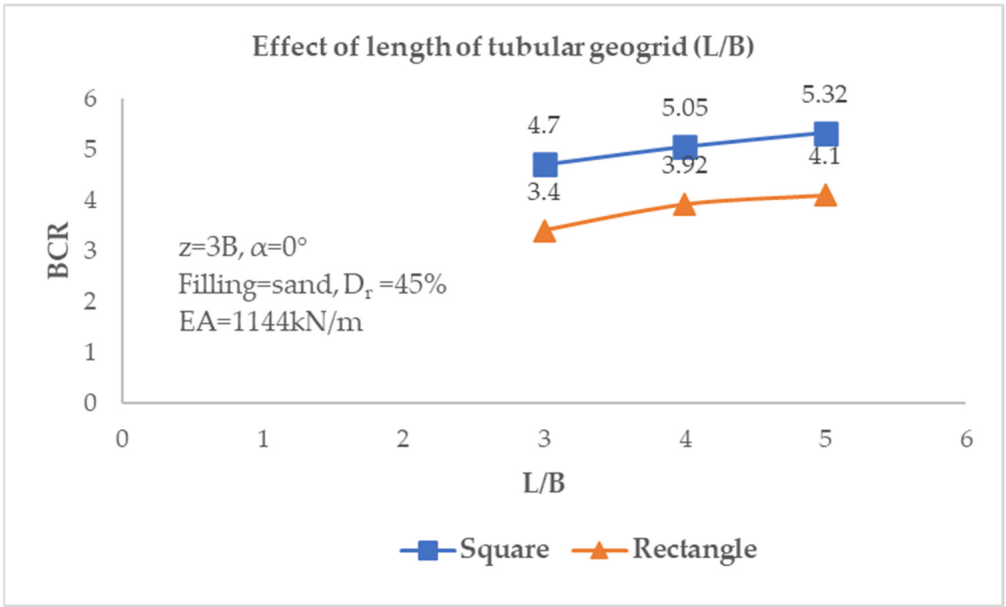


Figure 4. BCR versus L/B for square and rectangular footing.

4.4. The Impact of the Filler Inside the Tubular Geogrid

The effect of the filler material inside the tubular geogrid was analyzed by varying the filler between sand and aggregate. The other parameters were kept constant as z = 3 B,

$\alpha = 0°$, L = 4 B, D_r = 45%, and EA = 1144 kN/m. The maximum values were obtained for rectangular footing with coarse aggregates as the filler material, but the difference between sand and aggregate was marginal as shown in Figure 5, and it can be concluded that the most suitable filler can be chosen based on the site requirements.

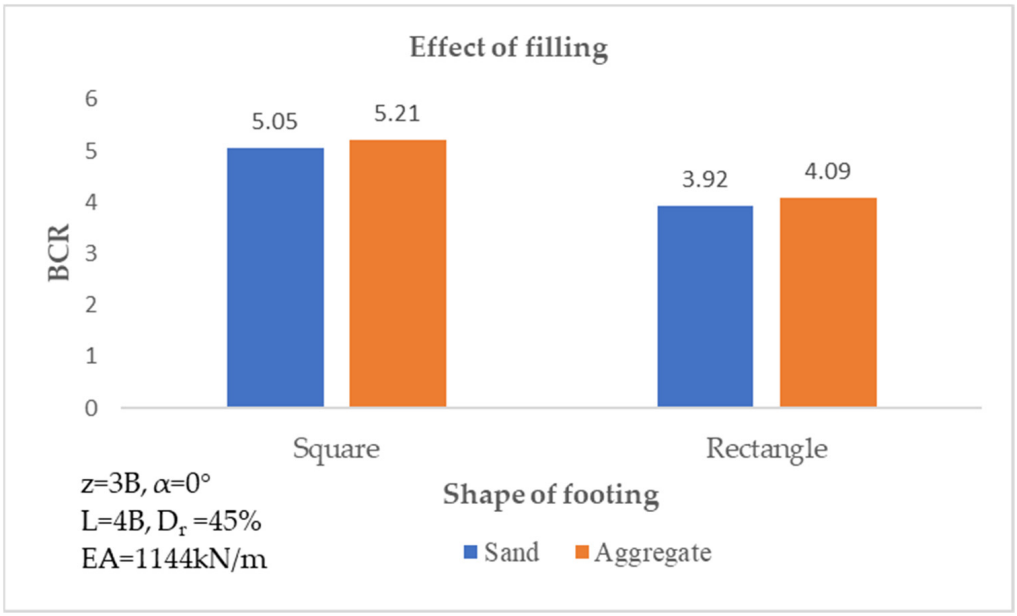


Figure 5. BCR versus shape of footing for varying filler materials.

4.5. Effect of Relative Density of Sand (D_r)

The effect of the relative density of the sand on the BCR of the soil is presented in Figure 6. The relative density was varied (30%, 45%, 60%, 75%, and 90%) while keeping the depth to the final layer of reinforcement, inclination, length, filling, and the tensile stiffness of the geogrid constant at 3 B, 0°, 4 B, sand, and 1144 kN/m, respectively. It can be observed from the graph that, as the relative density increases, the UBC also increases. The maximum increase was found for square footing with D_r = 90%, at 1178.72 kN/m^2. There are two ways in which the tubular geogrid offers vertical confinement: First, the friction between the tubular geogrid and the filling material. Secondly, the base reinforced with the tubular geogrid serves as a mattress to prevent soil from rising outside of the loading area. As the relative density increases, the sand grains dilate more, resulting in higher lateral confinement; this also increases the interface friction angle and stiffens the reinforced area. As a result, the curved surface increases the upward reaction and decreases the additional net stress on the soil substrate. The footing performance improves in more compacted sand because the geogrid layer's increased stiffness allows the footing pressure to disperse over a larger area and reduces the pressure imparted to the soil. Hence, for effective utilization of the reinforcement, the foundation soil should be compacted to a higher density [36].

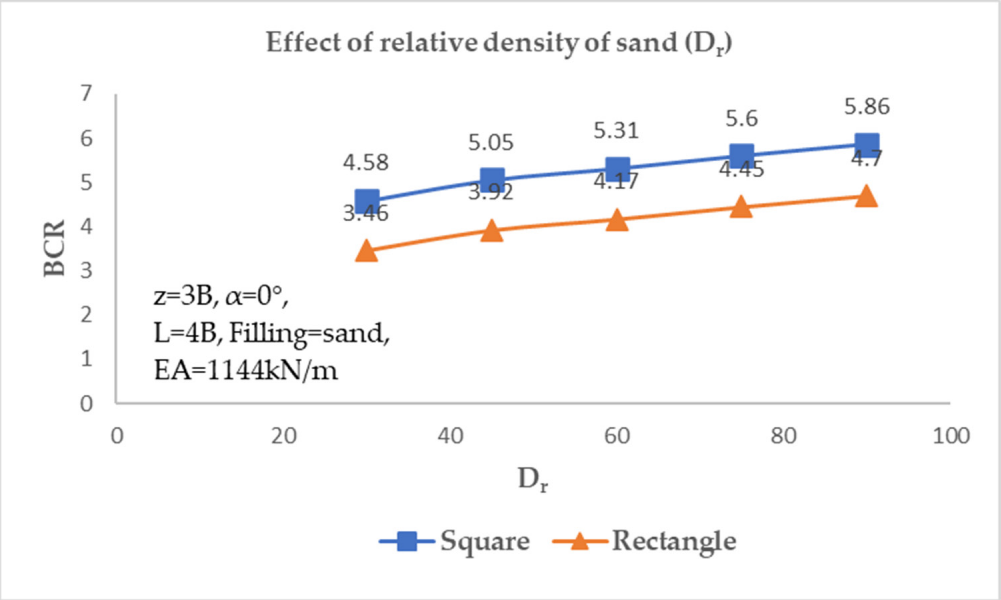


Figure 6. BCR versus D_r for square and rectangular footing.

4.6. The Effect of the Tensile Stiffness of the Geogrid (EA)

Figure 7 presents the variation in BCR with varying tensile stiffness (EA) of the geosynthetic reinforcement (500 kN/m, 800 kN/m, and 1144 kN/m). From the figure, it is clear that as the stiffness of the geogrid increases, the UBC also increases. The confinement of soil particles and the frictional resistance provided by the reinforcement both improve with increasing geogrid stiffness. The same trend was noted by [37,38].

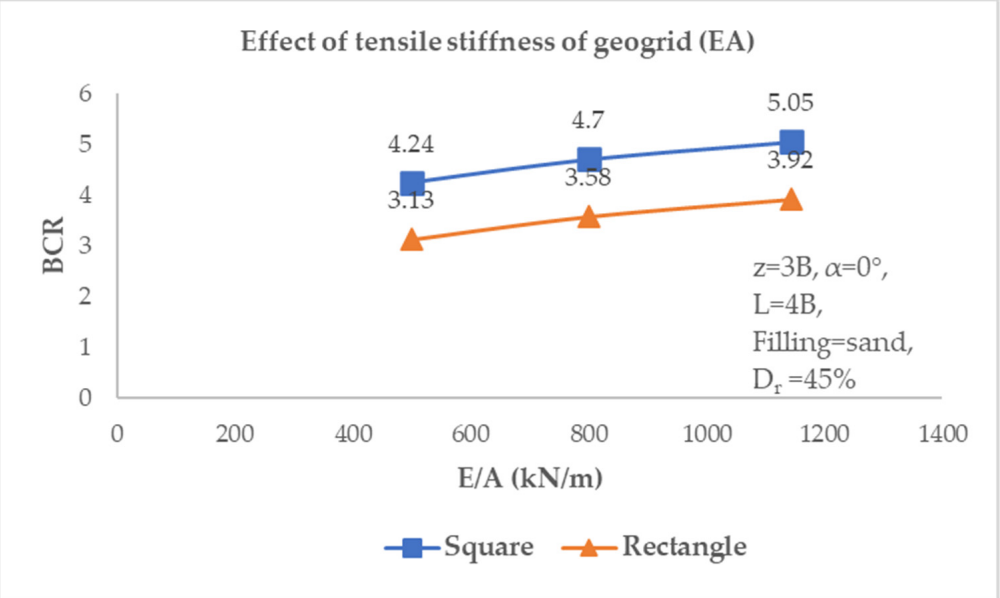


Figure 7. BCR versus EA for square and rectangular footing.

4.7. Verification

In this research, the results from experiments conducted in the laboratory were used for validation. River sand at proximity was used for the experimental setup. The soil was tested against the standards documented in the USCS (United Soil Classification System). The soil was classified as poorly graded sand (SP) and found to have a coefficient of uniformity (C_u), coefficient of curvature (C_c), effective grain size (D_{10}), and specific gravity (G) of 3.09, 1.15,

0.34 mm, and 2.65, respectively. Additionally, the angle of internal friction (ϕ) was noted as 35° at a relative density of 45%. A biaxial geogrid with a tensile strength of 31.5 kN/m in both the longitudinal and transverse directions was employed as the reinforcement material in this study. On the prepared sand bed, plate load tests were performed in a steel tank with internal measurements of 1.0 m × 0.60 m × 0.60 m, in accordance with IS 1888-1982 [39]. A 100 mm square plate and a 100 mm × 150 mm rectangular plate were used. The plate and the tank were chosen in such a way that the tank was five times as wide and deep as the footing; hence, the boundary effect was negligible [40]. Plate load tests were conducted for unreinforced sand beds and planar-reinforced sand beds.

To calibrate the software, several models were developed for the unreinforced and planar-reinforced cases, and trial runs were conducted and compared with the experimental results. Figure 8 depicts the results of this validation. From the figure, it can be observed that the numerical modeling results were in good agreement with the experimental results. Furthermore, to compare the results, the numerical tests were given the same specifications as the laboratory tests.

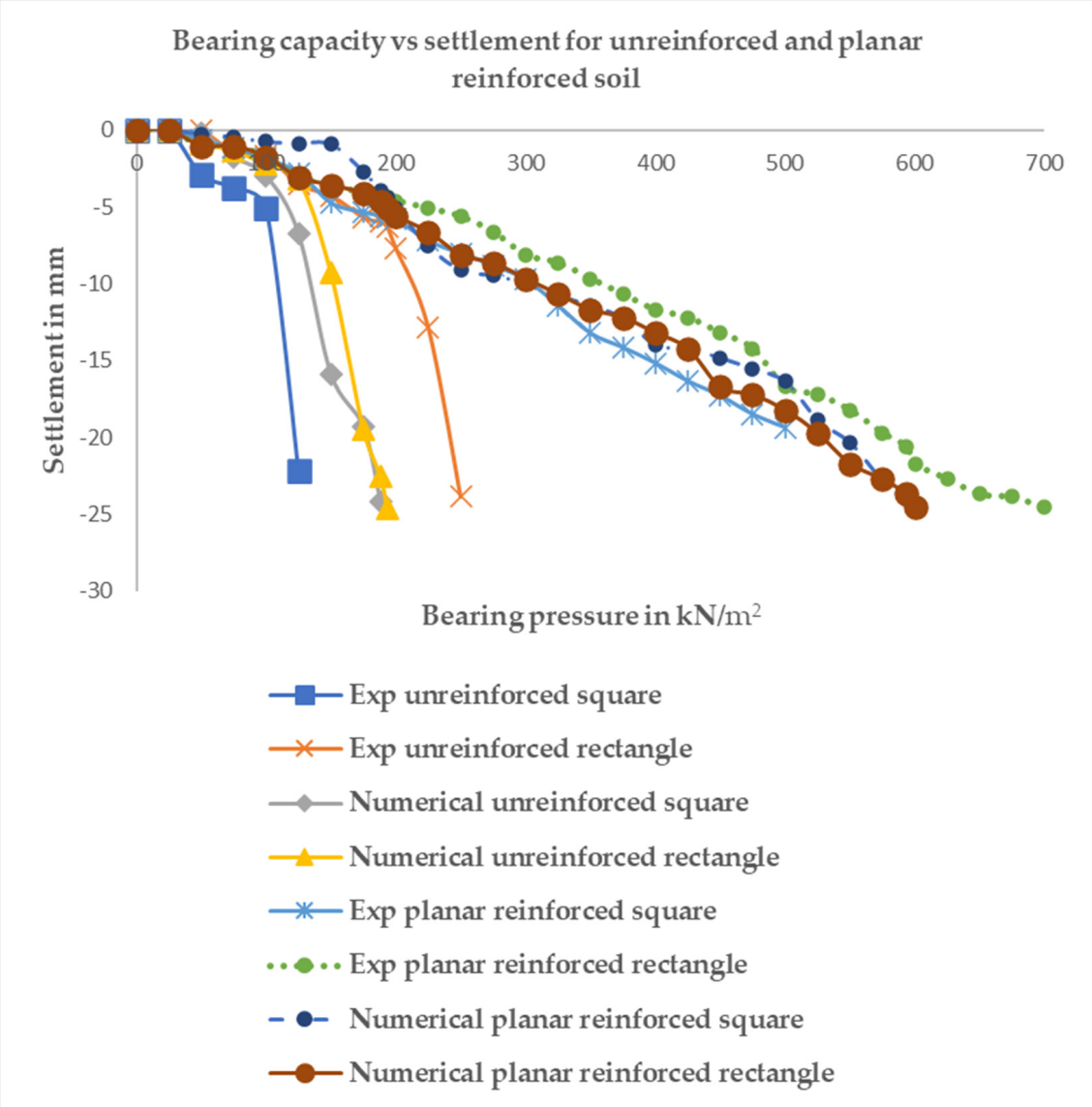


Figure 8. Comparison of experimental and numerical results.

5. AI-ML Techniques for Estimation of Ultimate Bearing Capacity

5.1. Dataset

The dataset was created based on the lab experiments and the PLAXIS-simulated experiments. A total of 348 experiments were conducted, 75% (261 recorded simulations) of which were used for training the model, while the remaining 25% (87 recorded simulations) were used for validation.

The predictors of the independent variables with the bearing capacity of the soil are provided below in Table 3 with their units and their statistical distribution in the training and validation datasets.

Table 3. Statistical properties of independent variables.

Variable	Unit	Train			Validation		
		Min	Mean	Max	Min	Mean	Max
Breadth (B)	m	100	125	150	100	125	150
Depth to breadth	Ratio	1.5	3	4.5	1.5	3	4.5
Length to breadth	Ratio	3	4	5	3	4	5
Alpha	Degree	0	40	120	0	0	120
Tensile modulus	kN/m	500	1017	1144	500	1045	1144
ϕ	Degree	32	36	41	32	36	41
Bearing capacity	kN/m^2	181.67	729.0	1212.3	180.67	761.27	1229.45

It was ensured that the split of the training and validation data did not affect the distribution of the data. In addition to the above statistics, correlation coefficients between the given variables were also calculated to check for multicollinearity, as presented in Figure 9; this is a serious problem in regression that can adversely affect the model training. To check for multicollinearity, we plotted the correlation coefficient and variance inflation factor (VIF), as given in Figure 10 and Table 4, respectively. Generally, a VIF of less than 5 is considered to be nominal, and the calculated values for different parameters were within desirable limits, showing no evidence for the presence of multicollinearity.

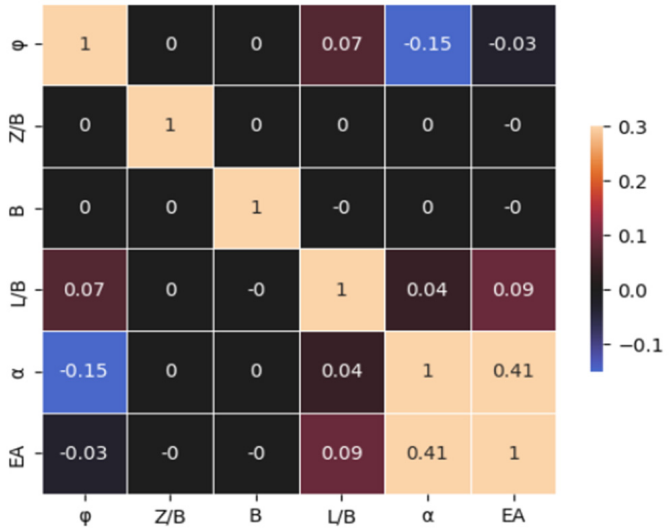


Figure 9. The correlation coefficients of all of the independent variables.

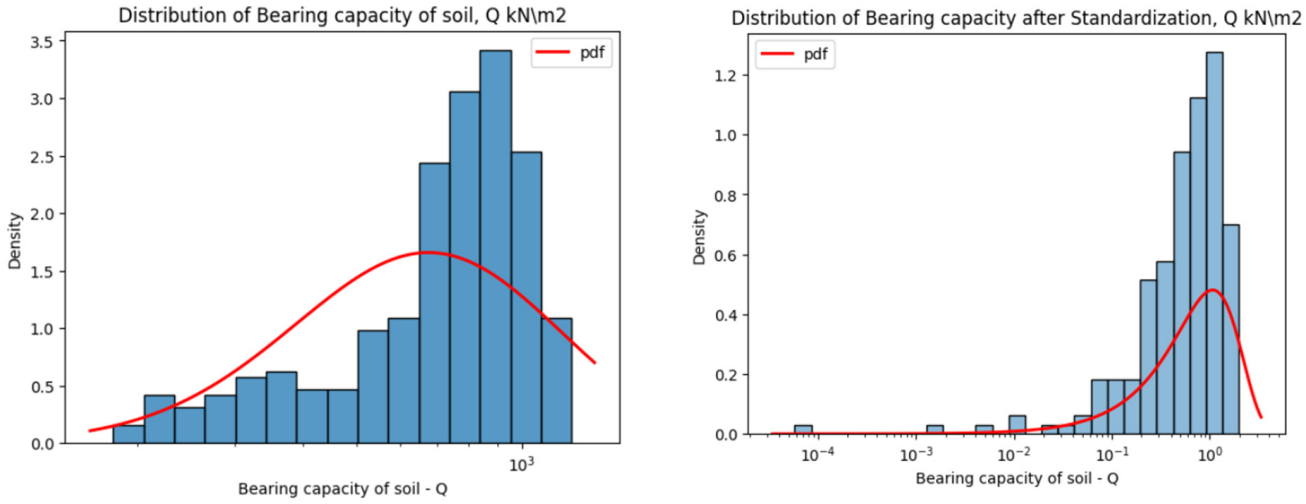


Figure 10. Histogram plot of bearing capacity.

Table 4. Variance inflation factors for all model variables.

Parameters	VIF
Φ	1.06
Z/B	1.00
α	1.23
B	1.00
L/B	1.01
Filler	1.15
EA	1.30

The histogram below (Figure 10) shows the distribution of the bearing capacity of the soil before and after standardization. A normality test based on the work of [41] was carried out, and the results were statistically significant, confirming that the data were not normally distributed. However, the ANN models are universal approximators and do not have any distribution-based assumptions, unlike linear regression models.

Table 4 shows the VIF values for the variables as part of the analysis. All of the values are close to one, indicating that the variances of the coefficients are not inflated at all.

$$VIF_j = \frac{1}{1 - R_j^2} \tag{1}$$

Equation (1) presents the formula for the variance inflation factor, where R_j is the R-squared value obtained by regressing the j^{th} predictor on the remaining predictors.

Apart from the univariate analysis, bivariate data analysis of the variation in bearing capacity with the other predictors was carried out to derive an understanding of the impacts of different variables, and the results are presented in Figure 11.

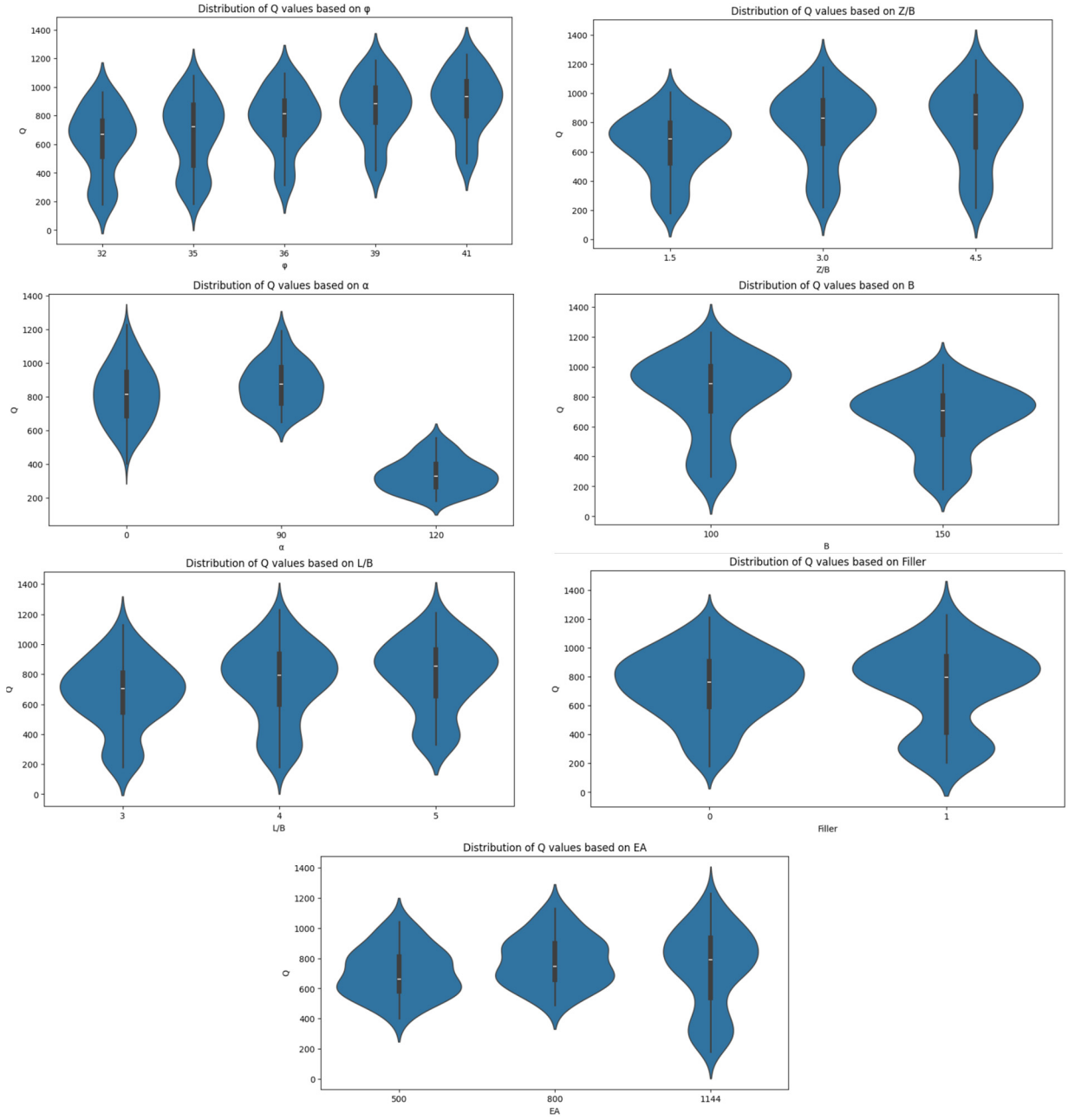


Figure 11. Violin plot of bearing capacity over different parameters.

5.2. Model Architecture and Comparison

In this study, we used three models from different paradigms of machine learning: (a) linear regression, (b) random forest, and (c) artificial neural networks. Linear regression has its foundation in classical statistical learning. Random forest is an ensemble method based on decision trees built using Gini impurity (information theory). Finally, artificial neural networks are recently popularized ML algorithms based on backpropagation learning techniques.

5.2.1. (a) Linear Regression Analysis

A linear regression model was developed based on all six features and with a constant term. While performing the analysis, the categorical value "Filler" was found to be insignificant based on the *p*-value and, hence, was removed from the model. The coefficient column in Table 5 shows the effect of unit change in each feature on the ultimate bearing

capacity of the soil. The corresponding standard errors and *p*-values are also provided, along with the confidence intervals of the coefficient of each feature.

Table 5. Output of linear regression model.

	Co−eff	***Std err***	***T***	***P>|t|***	**[0.025]**	**[0.975]**
Const	−429.3823	150.064	−2.861	0.005	−724.910	−133.855
ϕ	28.0257	3.438	8.151	0.000	21.255	34.797
Z/B	46.7820	7.953	5.882	0.000	31.120	62.444
α	−3.0902	0.204	−15.185	0.000	−3.491	−2.689
B	−2.8315	0.386	−7.330	0.000	−3.592	−2.071
L/B	54.6973	14.881	3.676	0.000	25.392	84.003
EA	0.2602	0.046	5.603	0.000	0.169	0.352
Filler	Removed after checking for *p*-value > 0.05					

The final equation of the ultimate bearing capacity of the soil, as determined by linear regression was

$$BC = -429.38 + 28.03\phi - 2.83B + 46.78\frac{Z}{B} + 54.7\frac{L}{B} - 3.10\alpha + 0.26\ EA \quad (2)$$

with an average error of 20.98% and R^2 = 61.7%

5.2.2. (b) Random Forest Model

Random forest is part of the ensemble model family, where several decision trees are built based on the "Gini impurity" index. Specifically, random forest is an ensemble method that uses bagging to reduce the bias of the estimate provided by a single decision tree, and this improves the model performance. We ensured diversity in the results generated by the trees by choosing features at random while building each decision tree. Meanwhile, this also helped us to understand the importance of each feature. An example of a decision tree is provided below in Figure 12.

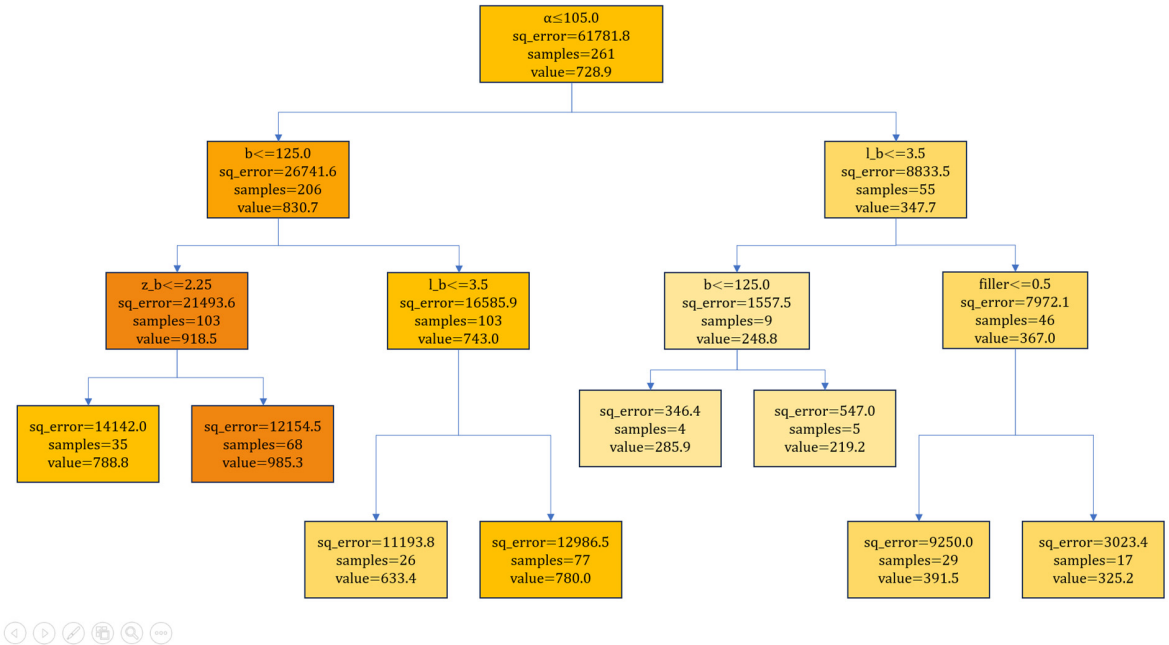


Figure 12. One of the decision trees as part of the random forest model.

The decision tree tries to find the key feature that divides the target space (UCB of soil) into a more homogeneous group, e.g., when $\alpha \leq 105$, the average value of UBC is high, i.e., 830.787, whereas when $\alpha > 105$, the average value of UBC is low, i.e., 347.707. Likewise, we created several nodes for each tree. Although this is an effective way to regress UBC over several features, it poses a threat of overfitting (the model tends to work well for the training data but poorly for validation data; the squared error for training data is low, while the squared error for validation data is high). This is not a favorable outcome; hence, once the entire tree is built, we can prune the tree to an optimal height such that the errors are low for both the training and validation datasets. We optimized several hyperparameters, including "max_depth", "max_leaf_nodes", and "min_samples_leaf", in order to avoid overfitting. The final chosen parameter values were max_depth = 3, max_leaf_nodes = 9, and min_samples_leaf = 26.

The feature importance also helps us to understand the relative information held by each feature for different UBC values of the soil. From Figure 13, we can infer that "alpha" is the most used feature as part of the nodes in the random forest, while "B" is the second most used, followed by "Z/B". Filler is the least informative feature. We came to the same conclusion in the linear regression.

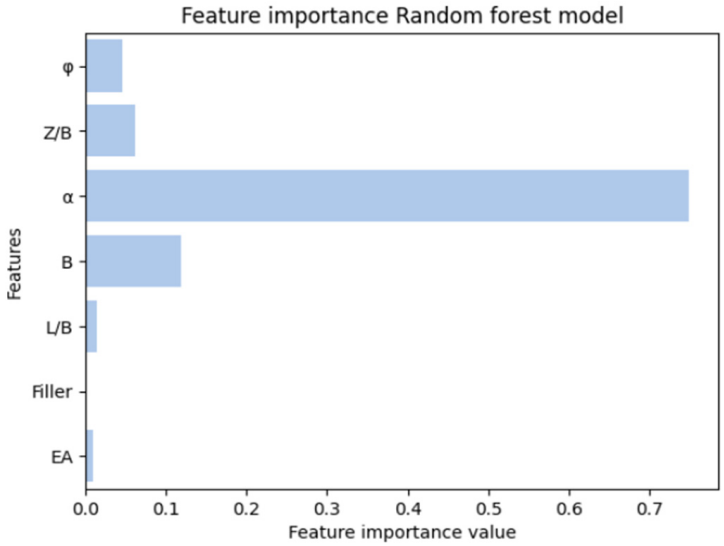


Figure 13. Feature importance depicted from the random forest model.

Table 6 presents the list of parameters that were experimented with, along with the final chosen values.

Table 6. Hyperparameter tuning conducted for the random forest model.

Parameters	Sampling Distribution	Final Chosen Value
Max_depth	Poisson with mean 2, shift 2	3
Max_leaf_nodes	Poisson with mean 2, shift 2	9
Min_samples_leaf	Uniform	26

The model achieved an average absolute error of 12.5%, with R^2 = 84.2%.

5.2.3. (c) Artificial Neural Network Model

A single hidden layer with a nonlinear activation function (ReLU) was trained using the backpropagation technique to predict the ultimate bearing capacity of the soil. The layout of the discussed ANN is depicted in Figure 14. The mean absolute error was 6.4%,

and the R^2 = 96.7%. The mean squared error was used as the loss function, which is a square of the error between predicted UBC and actual UBC.

$$Loss\ function\ := Mean\ squred\ error\ := \frac{1}{n}\sum_{i=1}^{n}\left(Y_i - \hat{Y}_i\right)^2 \quad (3)$$

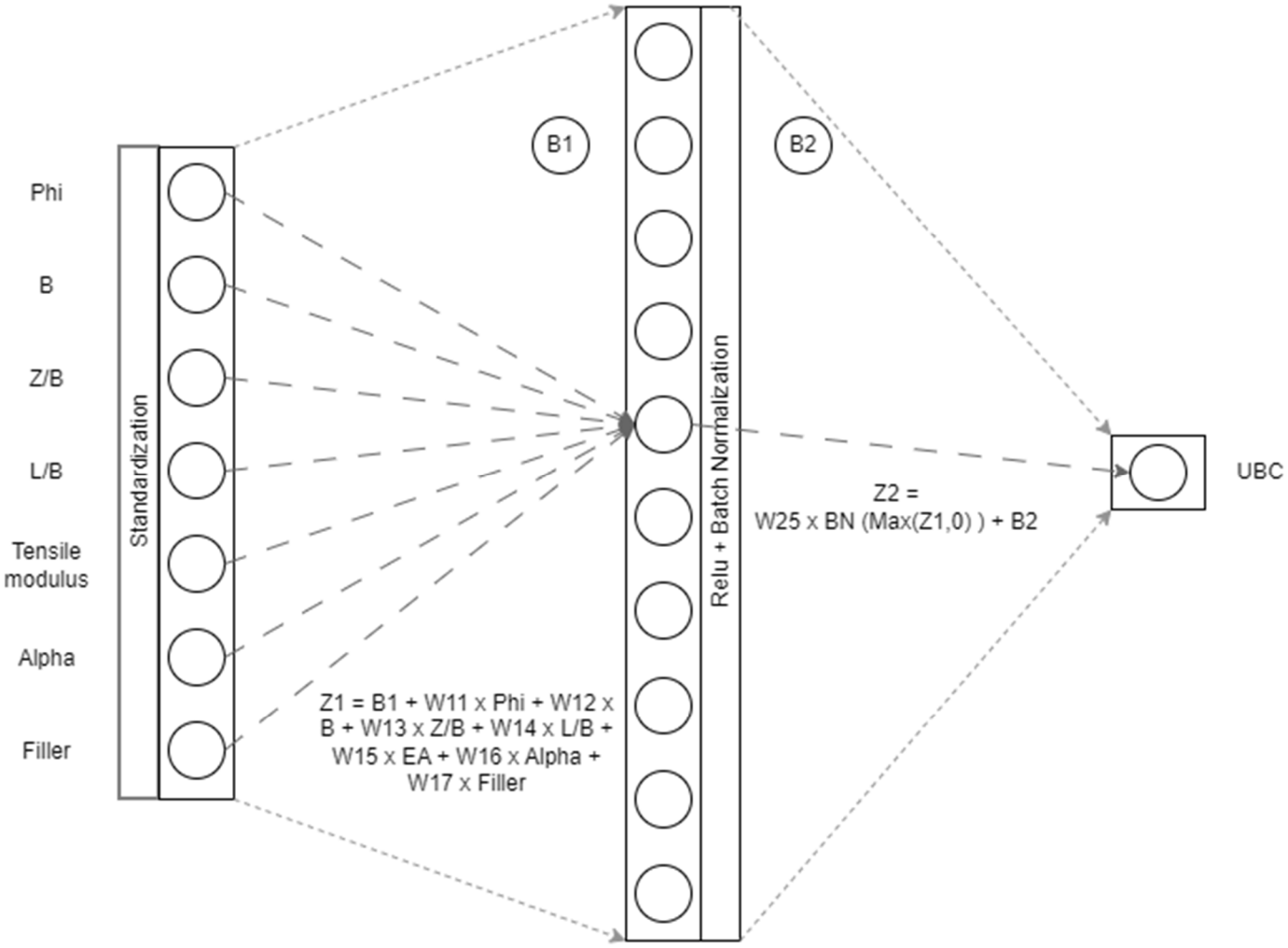


Figure 14. Representation of neural network.

Here, Y_i is the actual UBC, $\hat{Y}_i$ is the predicted UBC, and n is the total number of samples in the batch.

A batch normalization layer was introduced in between the hidden layer and the final output layer, in order to improve the stability of the model training. The input features were also normalized before training, in order to ensure faster convergence. The training process was monitored to check for signs of overfitting, of which no evidence was found.

Once the training was complete, the model weights were frozen and saved separately for prediction. The first layer contained weights of dimensions 7×10 since the total number of variables was seven and the number of neurons in the hidden layer was 10, while the bias values were 10.

Similarly, there were 10 neurons in the hidden layer and one output layer; the weights of the second layer were 10×1, with a single bias. All of the values are provided in Table 7.

Table 7. The weights and biases of the model.

	Neuron 1	Neuron 2	Neuron 3	Neuron 4	Neuron 5	Neuron 6	Neuron 7	Neuron 8	Neuron 9	Neuron 10
Layer 1 weights	0.06775	−0.00118	−0.12457	−0.00855	0.112256	0.00373	0.013384	0.002035	0.082196	0.001254
	0.049655	0.015973	−0.06399	0.002026	0.022351	−0.00366	0.039188	0.09085	−0.00796	0.011926
	−0.01257	0.20013	0.030993	0.161962	−0.0074	−0.0432	0.068996	−0.01131	0.007179	0.203202
	0.017555	−0.00859	0.032284	−0.00443	−0.03402	−0.10191	−0.01762	−0.11718	0.031619	−0.00978
	0.071894	0.001777	−0.12005	0.002597	0.034712	0.002353	0.009694	−0.00438	0.016757	0.001773
	−0.01713	0.003529	0.028349	0.014182	−0.02765	0.001425	0.026858	0.000574	0.061525	0.003709
	0.000572	−0.11888	−0.00398	−0.11926	0.042799	−0.0048	−0.00411	−0.00143	0.070369	−0.10271
Layer 1 bias	−0.03008	−0.16454	0.017542	−0.09721	0.057369	0.010442	0.178682	−0.00782	0.115483	−0.17836
Layer 2 weights	0.049437	−0.2421	−0.10662	−0.21922	0.110227	0.188325	0.200743	0.173094	0.120177	−0.41183
Layer 2 bias	0.00493933									
Batch norm										
Gamma weights	0.94626	1.392452	1.093512	1.330648	1.14541	1.109567	1.270016	1.104237	1.175961	1.539068
Beta weights	0.004797	0.01433	−0.00337	0.023141	−0.02415	0.004808	0.000171	0.005538	0.004744	−0.005789
Moving mean	0.0319	0.019426	0.091684	0.026688	0.083677	0.057636	0.177104	0.055077	0.129952	0.01781
Moving variance	0.00252	0.001298	0.013062	0.001336	0.009112	0.003803	0.006983	0.005827	0.010161	0.001084

A closed-form formula was developed from the weights and bias extracted from the model and substituted into the equation given below [42]:

Inputs:

$$X = \left[\phi, \frac{z}{b}, \alpha, B, \frac{L}{B}, Filler, EA\right], \mathbb{R}^{1X7} \quad (4)$$

Parameters:

$$W_1 = Weights\ of\ layer\ 1, \mathbb{R}^{10x7}$$

$$B_1 = Bias\ of\ layer\ 1, \mathbb{R}^{10x1}$$

$$W_2 = Weights\ of\ layer\ 2, \mathbb{R}^{10x1}$$

$$B_2 = bais\ of\ layer\ 2, \mathbb{R}^{1x1}$$

$$\gamma, \beta = parameter\ of\ batch\ normalization\ learnt\ while\ training, \mathbb{R}^{10x1}$$

$$mu_{mov}, \sigma_{mov} = Moving\ mean\ and\ std\ deviation\ learnt\ while\ training, \mathbb{R}^{10x1}$$

$$Z_1' = Output\ of\ the\ 1st\ layer, \mathbb{R}^{10x1}$$

$$Z_2 = Model\ predictions, \mathbb{R}^{1x1}$$

Layer 1:

$$Z_1 = Max\left(W_1 x X^T + B_1, 0\right)$$

$$Z_1' = \gamma \odot \frac{(Z_1 - \mu_{mov})}{\sigma_{mov}} + \beta$$

Layer 2:

$$Z_2 = W_2 x \left(Z_1'\right)^T + B_2$$

5.3. Results and Discussion

All three AI-ML models were built to predict the ultimate bearing capacity using the given seven specific features. These features and their values were determined through laboratory studies and PLAXIS-based simulations. The performance metrics are listed in Table 8 below, and the model training vs. validation loss curve is given in Figure 15.

Table 8. Comparison of metrics for different AI models.

Technique		MSE	MAE	MAPE	R^2	RMSE
Formula		$\frac{1}{n}\sum_{i=1}^{n}(Y_i-\hat{Y}_i)^2$	$\frac{1}{n}\sum_{i=1}^{n}\lvert Y_i-\hat{Y}_i\rvert$	$\frac{1}{n}\sum_{i=1}^{n}\frac{\lvert Y_i-\hat{Y}_i\rvert}{Y_i}$	$1-\frac{\sum_{i=1}^{n}(Y_i-\hat{Y}_i)^2}{\sum_{i=1}^{n}(Y_i-\overline{Y_i})^2}$	$\sqrt{[\frac{1}{n}\sum_{i=1}^{n}(Y_i-\hat{Y}_i)^2]}$
Linear regression	Train	153.75	118.72	20.98%	61.74%	12.4
	Test	170.36	130.57	20.38%	53.23%	13.05
Random forest	Train	93.63	74.15	10.97%	85.8%	9.68
	Test	99.06	79.48	12.5%	84.18%	9.95
Artificial neural network	Train	45.14	36.14	6.4%	96.7%	6.72
	Test	53.7	44.87	8.26%	95.35%	7.33

Note: Train and test values are provided in the table for each technique; Y_i = actual UCB, and $\hat{Y}_i$ = predicted UBC.

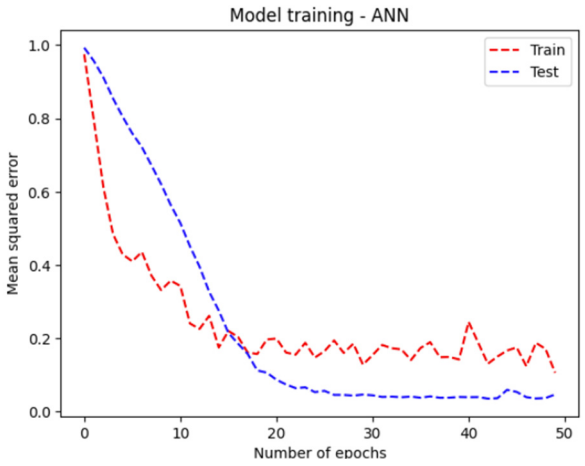


Figure 15. Model training vs. validation loss curve.

From the performance metrics in Table 8 and the model prediction graphs, it is clear that, for this particular case, the ANN model gives better predictions, with no overfitting and a low error rate. In the predicted vs. actual graph (Figure 16) of the ANN model, it can be observed that the thicker band formed around the 45° line, showing that the difference between the error is consistently low and centered around zero. This also shows that the output of the model is stable and reliable.

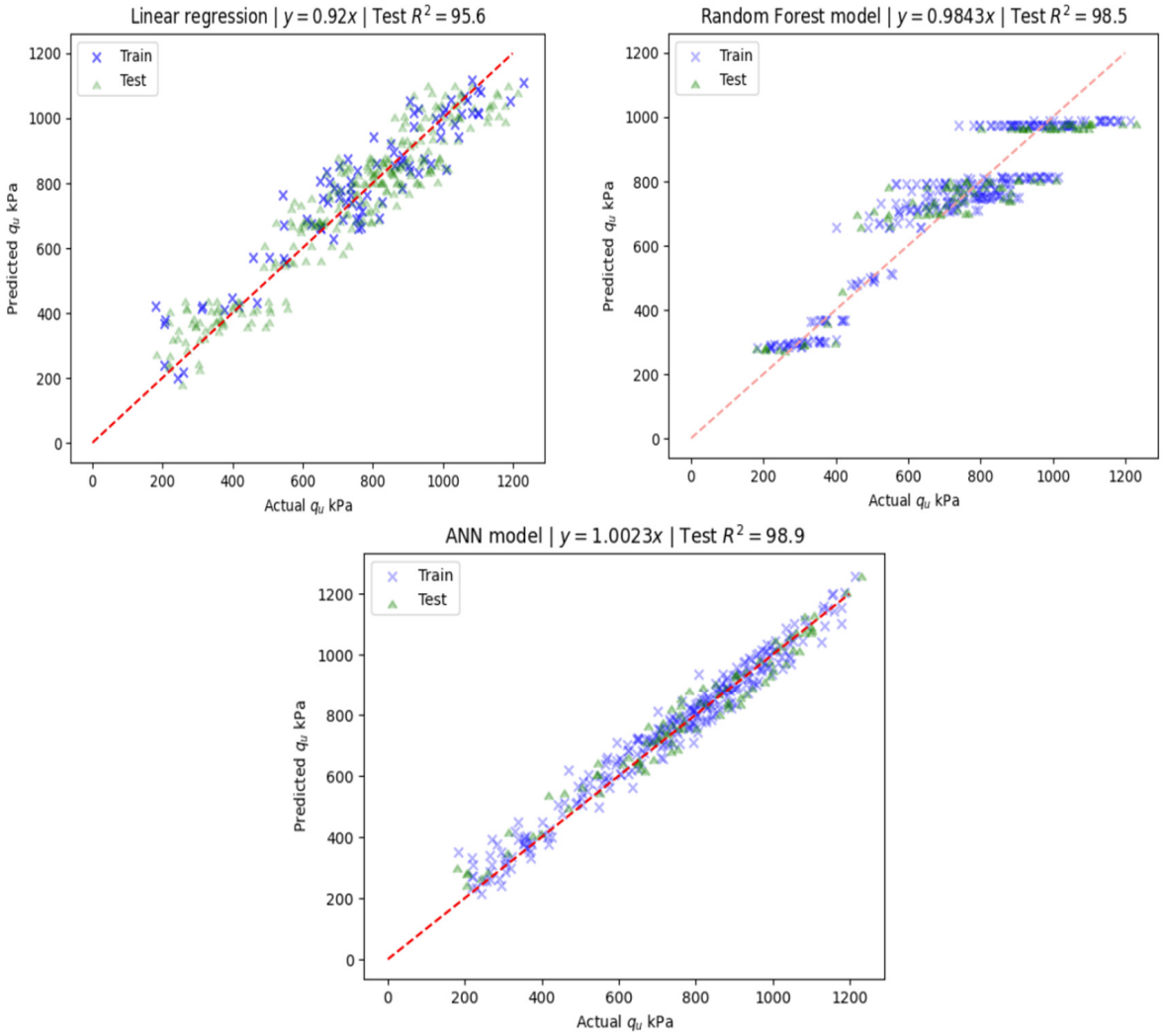


Figure 16. Actual vs. predicted plot with R^2 values.

6. Conclusions

The various conclusions drawn from this study are as follows:

1. The use of 3D tube geogrids as reinforcement increased the confinement effect between the soil and the geogrid, thus aiding in increasing the bearing capacity. As the depth of the final layer increases, the bearing capacity also increases, and the optimal depth was found to be 3 B. Increasing the depth to more than 3 B did not have much effect on the bearing capacity. When the inclination of the geogrid was 0° and 90 °, the bearing capacity value did not show much difference, but when it was 120°, the bearing capacity decreased. The optimal length of the tubular geogrid was found to be 4 B. As the inside of the tubular geogrid was filled with aggregates, the bearing capacity increased when compared to that of the sand, but this increase was not significant.
2. Three different types of AI techniques were used for this study: a linear regression model, a random forest model, and an artificial neural network. The absolute percentage error for the ANN model was found to be 42% less than that of the next-best model (i.e., the random forest model). This shows that the ANN was effective in estimating the bearing capacity of the soil more accurately. The usage of these AI techniques gives an advanced resolution in predicting the bearing capacity of footing on reinforced sand beds in a simple and economic manner. In comparison with the conventional methods, these techniques provide better accuracy and efficiency.

7. Limitations and Future Work

In order to obtain more precise findings, these tests and simulations should be repeated using larger-scale models, as the tests carried out in this research were performed on a scaled-down model, and the materials did not behave exactly how they do in reality.

Author Contributions: Data curation, P.A.J.; formal analysis, P.A.J.; funding acquisition, P.A.J.; methodology, M.M.; project administration, M.M.; software, P.A.J.; supervision, M.M.; validation, P.A.J.; writing—original draft, P.A.J.; writing—review and editing, M.M. All authors have read and agreed to the published version of the manuscript.

Funding: This work was supported by the Center for Research—Anna Centenary Research Fellowship-2020 [CFR/ACRF-2020/AR1,2020] by Anna University, Chennai.

Data Availability Statement: The data that support the findings of this study are available from the corresponding author upon reasonable request.

Conflicts of Interest: The authors have no competing interests to declare that are relevant to the content of this article.

References

1. Abu-Farsakh, M.; Chen, Q.; Sharma, R. An experimental evaluation of the behavior of footings on geosynthetic-reinforced sand. *Soils Found.* **2013**, *53*, 335–348. [CrossRef]
2. Tafreshi SN, M.; Khalaj, O.; Dawson, A.R. Pilot-scale load tests of a combined multilayered geocell and rubber-reinforced foundation. *Geosynth. Int.* **2015**, *20*, 143–161. [CrossRef]
3. Venkateswarlu, H.; Ujjawal, K.N.; Hegde, A. Laboratory and numerical investigation of machine foundations reinforced with geogrids and geocells. *Geotext. Geomembr.* **2018**, *46*, 882–896. [CrossRef]
4. Al-Subari, L.; Hanafi, M.; Ekinci, A. Effect of geosynthetic reinforcement on the bearing capacity of strip footing on sandy soil. *SN Appl. Sci.* **2020**, *2*, 1484. [CrossRef]
5. Buragadda, V.; Thyagaraj, T.; Dhiman, R.; Orekanti, E.R.; Maddileti, T.K. Influence of Geosynthetic Reinforcement Geometrical Parameters on Load-Bearing Capacity of Sand: An Experimental Study. *Transp. Infrastruct. Geotechnol.* **2024**, 1–27. [CrossRef]
6. Giroud, J.P. Quantification of geosynthetic behavior. *Geosynth. Int.* **2005**, *12*, 2–27. [CrossRef]
7. Hossain, M.B.; Hossain, M.Z.; Sakai, T. Interaction Properties of Geosynthetic with Different Backfill Soils. *Int. J. Geosci.* **2012**, *3*, 1033–1039. [CrossRef]
8. Mcgown, A. *The Behaviour of Geosynthetic Reinforced Soil Systems in Various Geotechnical Applications*; University of Strathclyde: Glasgow, UK, 2000; pp. 3–23.
9. Palmeira, E.M. Soil–geosynthetic interaction: Modelling and analysis. *Geotext. Geomembr.* **2009**, *27*, 368–390. [CrossRef]
10. Pinho-Lopes, M.; Paula, A.M.; Lopes, M.L. Soil–geosynthetic interaction in pullout and inclined-plane shear for two geosynthetics exhumed after installation damage. *Geosynth. Int.* **2016**, *23*, 331–347. [CrossRef]
11. Raja MN, A.; Shukla, S.K. Ultimate bearing capacity of strip footing resting on soil bed strengthened by wraparound geosynthetic reinforcement technique. *Geotext. Geomembr.* **2020**, *48*, 867–874. [CrossRef]
12. Shaikh, S.I.; Awachat, D.B.; Dhatrak, A.I. Experimental Investigation on Machine Foundation Resting on Reinforced Sand Bed. Isteonline. Available online: http://isteonline.in/Datafiles/cms/IJTE%20Journal%20Apr%20to%20June%202023%20web.pdf#page=54 (accessed on 13 July 2024).
13. Shil, T.; Pal, S.K. Behaviour of geocomposite and geotextile reinforced soil bed—An experimental study. *Mater. Today Proc.* 2023; *in press*. [CrossRef]
14. Waleed, A.A.; Selçuk, M.E.; Mohsen, M.K. Investigation behavior of gypsum soil reinforced by geosynthetics supported square footing-an experimental study. *IOP Conf. Ser. Earth Environ. Sci.* **2023**, *1232*, 012063. [CrossRef]
15. Gupta, S.; Mital, A. A comparative study of bearing capacity of shallow footing under different loading conditions. *Geomech. Geoengin.* **2022**, *17*, 1338–1349. [CrossRef]
16. Abdolhosseinzadeh, A.; Samui, P.; Samaei, M.; Garousi, A. Numerical analysis of bearing capacity of circular footing reinforced with geogrid layers. *Arab. J. Geosci.* **2022**, *15*, 750. [CrossRef]
17. Kazi, M.; Shukla, S.K.; Habibi, D. An Improved Method to Increase the Load-Bearing Capacity of Strip Footing Resting on Geotextile-Reinforced Sand Bed. *Indian Geotech. J.* **2015**, *45*, 98–109. [CrossRef]
18. Latha, G.M.; Somwanshi, A. Bearing capacity of square footings on geosynthetic reinforced sand. *Geotext. Geomembr.* **2009**, *27*, 281–294. [CrossRef]
19. Kazi, M.; Shukla, S.K.; Habibi, D. Behaviour of an embedded footing on geotextile-reinforced sand. *Proc. Inst. Civ. Eng.-Ground Improv.* **2016**, *169*, 120–133. [CrossRef]
20. Lovisa, J.; Shukla, S.K.; Sivakugan, N. Behaviour of prestressed geotextile-reinforced sand bed supporting a loaded circular footing. *Geotext. Geomembr.* **2010**, *28*, 23–32. [CrossRef]

21. Salari, M.; Lezgy-Nazargah, M.; Shafaie, V.; Rad, M.M. Numerical Study of the Ultimate Bearing Capacity of Two Adjacent Rough Strip Footings on Granular Soil: Effects of Rotational and Horizontal Constraints of Footings. *Buildings* **2024**, *14*, 1653. [CrossRef]
22. Dey, A.; Basudhar, P.K. Bearing Capacity of Surface Footings on Reinforced Sandy Bed: A Revised Regression Model. *Indian Geotech. J.* **2021**, *52*, 448–462. [CrossRef]
23. Doley, C.; Das, U.K.; Shukla, S.K. Development of a multiple regression equation for prediction of bearing capacity of geocell-reinforced sand beds based on experimental study. *Arab. J. Geosci.* **2022**, *15*, 1408. [CrossRef]
24. Harandizadeh, H.; Jahed Armaghani, D.; Khari, M. A new development of ANFIS–GMDH optimized by PSO to predict pile bearing capacity based on experimental datasets. *Eng. Comput.* **2021**, *37*, 685–700. [CrossRef]
25. Misir, G.; Laman, M. A modern approach to estimate the bearing capacity of layered soil. *Period. Polytech. Civ. Eng.* **2017**, *61*, 434–446. [CrossRef]
26. Pham, T.A.; Vu, H.L.T.; Duong, H.A.T. Improving deep neural network using hyper-parameters tuning in predicting the bearing capacity of shallow foundations. *J. Appl. Sci. Eng.* **2022**, *25*, 261–273. [CrossRef]
27. Sultana, P.; Dey, A.K.; Kumar, D. Empirical approach for prediction of bearing pressure of spread footings on clayey soil using artificial intelligence (AI) techniques. *Results Eng.* **2022**, *15*, 100489. [CrossRef]
28. Yong, W.; Zhou, J.; Jahed Armaghani, D.; Tahir, M.M.; Tarinejad, R.; Pham, B.T.; Van Huynh, V. A new hybrid simulated annealing-based genetic programming technique to predict the ultimate bearing capacity of piles. *Eng. Comput.* **2021**, *37*, 2111–2127. [CrossRef]
29. Ebid, A.M.; Onyelowe, K.C.; Arinze, E.E. Estimating the Ultimate Bearing Capacity for Strip Footing Near and within Slopes Using AI (GP, ANN, and EPR) Techniques. *J. Eng.* **2021**, *2021*, 3267018. [CrossRef]
30. Raja, M.N.A.; Shukla, S.K. Predicting the settlement of geosynthetic-reinforced soil foundations using evolutionary artificial intelligence technique. *Geotext. Geomembr.* **2021**, *49*, 1280–1293. [CrossRef]
31. Harikumar, M.; Sankar, N.; Chandrakaran, S. Behaviour of model footing resting on sand bed reinforced with multi-directional reinforcing elements. *Geotext. Geomembr.* **2016**, *44*, 568–578. [CrossRef]
32. Moayedi, H.; Abdullahi, M.M.; Nguyen, H.; Rashid, A.S.A. Comparison of dragonfly algorithm and Harris hawks optimization evolutionary data mining techniques for the assessment of bearing capacity of footings over two-layer foundation soils. *Eng. Comput.* **2021**, *37*, 437–447. [CrossRef]
33. Chakraborty, M.; Kumar, J. Bearing capacity of circular foundations reinforced with geogrid sheets. *Soils Found.* **2014**, *54*, 820–832. [CrossRef]
34. El Sawwaf, M.; Nazir, A.K. Behavior of repeatedly loaded rectangular footings resting on reinforced sand. *Alex. Eng. J.* **2010**, *49*, 349–356. [CrossRef]
35. Tavangar, Y.; Shooshpasha, I. Experimental and Numerical Study of Bearing Capacity and Effect of Specimen Size on Uniform Sand with Medium Density, Reinforced with Nonwoven Geotextile. *Arab. J. Sci. Eng.* **2016**, *41*, 4127–4137. [CrossRef]
36. Dash, S.K. Influence of Relative Density of Soil on Performance of Geocell-Reinforced Sand Foundations. *J. Mater. Civ. Eng.* **2010**, *22*, 533–538. [CrossRef]
37. Marandi, S.M.; Bagheripour, M.H.; Rahgozar, R.; Ghirian, A.R. Numerical Investigation into the Behavior of Circular Pad Shallow Foundations Supported by Geogrid Reinforced Sand. *Am. J. Appl. Sci.* **2008**, *5*, 355–368. [CrossRef]
38. Merry, S.; Li, C.; Lawton, E. Performance of spread footings on subgrades reinforced with geogrids and geojacks. In Proceedings of the Geosynthetics '99: Specifying Geosynthetics and Developing Design Details, Boston, MA, USA, 28–30 April 1999.
39. *IS: 1888–1982, I.S*; Method of Load Test on Soils, Second Revision. Indian Standards Institution: New Delhi, India, 1982.
40. Mandal, J.N.; Sah, H.S. Bearing capacity tests on geogrid-reinforced clay. *Geotext. Geomembr.* **1992**, *11*, 327–333. [CrossRef]
41. D'Agostino, R.B. An Omnibus Test of Normality for Moderate and Large Size Samples. *Biometrika* **1971**, *58*, 341. [CrossRef]
42. Nguyen, T.H.; Nguyen, T.; Truong, T.T.; Doan DT, V.; Tran, D.H. Corrosion effect on bond behavior between rebar and concrete using Bayesian regularized feed-forward neural network. *Structures* **2023**, *51*, 1525–1538. [CrossRef]

Disclaimer/Publisher's Note: The statements, opinions and data contained in all publications are solely those of the individual author(s) and contributor(s) and not of MDPI and/or the editor(s). MDPI and/or the editor(s) disclaim responsibility for any injury to people or property resulting from any ideas, methods, instructions or products referred to in the content.